analytical chemistry

pubs.acs.org/ac Article

NMR Spectral Editing, Water Suppression, and Dipolar Decoupling in Low-Field NMR Spectroscopy Using Optimal Control Pulses and Multiple-Pulse Sequence

Ahmed Bahti,* Ahmad Telfah, Roland Hergenröder, and Dieter Suter*

Cite This: *Anal. Chem.* 2025, 97, 1983−1991 Read Online

ACCESS | Metrics & More | Article Recommendations | Supporting Information

ABSTRACT: Spectral dispersion in low-field nuclear magnetic resonance (NMR) can significantly affect NMR spectral analysis, particularly when studying complex mixtures like metabolic profiling of biological samples. To address signal superposition in these spectra, we employed spectral editing with selective excitation pulses, proving it to be a suitable approach. Optimal control pulses were implemented in low-field NMR and demonstrated their capability to selectively excite and eliminate specific amino acids, such as phenylalanine and taurine, either individually or simultaneously. The broadening of NMR signals in viscous samples, like bio samples, due to homonuclear dipolar coupling often leads to loss of spectral details, impacting spectral assignments. Therefore, in this work, the multiple-pulse WAHUHA sequence at both high and low field NMR was employed resulting in approximately 63 and 25% reduction in line widths respectively, evident from line width changes in the NMR spectra. The effectiveness of this process was validated by comparing its performance with that of magic angle spinning NMR. Additionally, water suppression was achieved through selective excitation by adding a term representing the water signal to the overall Hamiltonian, expressing the water signal peak frequency, and covering adjacent frequencies on both sides of the water peak within the water signal.

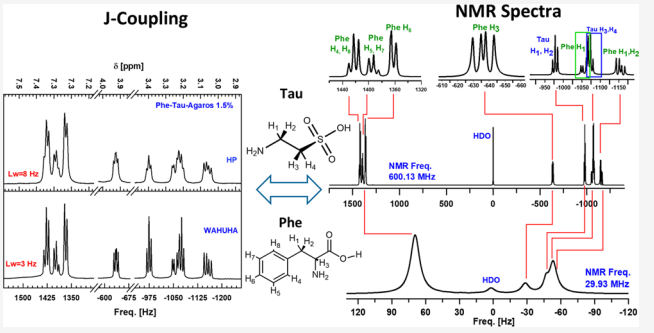

Low-field nuclear magnetic resonance (NMR) spectroscopy has gained considerable attention for analyzing physical, chemical, and structural properties of small molecules, lipids, and rigid solids.[1−13] Low-field nuclear magnetic resonance (NMR) is typically defined by magnetic field strengths below 2 T, corresponding to proton NMR frequencies below 85 MHz. Various classifications across literature specify different ranges within this definition. Some sources,[14−16] define low-field NMR as having frequencies below 42 MHz, while others extend the range up to 85 MHz.[17] The most common operational ranges for low-field NMR systems lie between 4 and 85 MHz, providing reduced spectral resolution and sensitivity compared to high-field systems but still suitable for applications in portable instrumentation, educational tools, and specific industrial processes.[18,19] Low-Filed NMR application for molecular assignment and quantification in complex biological mixtures, like biofluids and soft tissue samples, is hindered by low spectral dispersion.[20] To address signal superposition in NMR studies, techniques like pure shift NMR and diffusion ordered spectroscopy (DOSY) have been developed.[21−23]

Optimal control theory, a powerful tool for designing selective radio frequency pulses,[24,25] offers a promising solution for spectral editing and overcoming signal superposition in low-field NMR spectroscopy.[26−31] The implementation of Krotov-based optimal control pulses has resulted in converged selective excitation approaches for large spin systems, effectively suppressing unwanted spectral components. This method also leads to a reduction in algorithmic complexity, achieving a monotonically enhanced objective functional.[27,28] making it an effective approach for enhancing the resolution of low-field NMR experiments. Additionally, NMR pulses can be designed using the Krotov-based algorithm, as described in[30,31] and implemented using Matlab code from Maximov et al.,[27] based on Tannor et al.'s formulation.

High-resolution NMR spectra of biological tissues and viscous fluids face challenges due to inhomogeneous macroscopic magnetic susceptibility and large dipolar couplings among protons.[32,33] NMR signal broadening occurs due to the viscous nature of body fluids, resulting in incomplete averaging

Received: November 18, 2023
Revised: January 3, 2025
Accepted: January 4, 2025
Published: January 22, 2025

https://doi.org/10.1021/acs.analchem.3c05226
Anal. Chem. 2025, 97, 1983−1991

of dipole−dipole couplings.[34] In a homogeneous solution, the rapid reorientation of small molecules allows them to sample all orientations, resulting in an average dipole−dipole coupling of zero. However, this is not the case in viscous samples like biological samples.[35] Techniques like magic angle spinning (MAS) and homonuclear dipolar decoupling have been used to reduce line widths caused by dipolar couplings.[36−40] In this approach, the sample undergoes rapid rotation around an axis tilted at 54.74° with respect to the static magnetic field, However, these methods may require specialized hardware and can compromise sample integrity.[41,42] It necessitates dedicated hardware and specialized sample holders, namely zirconia rotors and Teflon disposable sample container.[43] Furthermore, the rapid spinning of biological tissue samples in high-resolution magic-angle-spinning (HR-MAS) can compromise sample integrity, making it difficult to study intact samples.[44] Besides MAS, homonuclear dipolar coupling can be mitigated using a sequence of four $\pi/2$ pulses known as the weak amplitude unmodulated homonuclear average (WAHUHA) pulse sequence. Unlike MAS, the WAHUHA approach for dipolar decoupling does not necessitate spinning or specialized hardware.[45] Implementing the WAHUHA pulse sequence can reduce broadening by 15−20%, which proves beneficial for viscous samples and biological tissues.[46] This study introduces the multiple-pulse WAHUHA sequence in both high and low field NMR, effectively eliminating dipolar terms in the average spin Hamiltonian up to the first-order.[47,48]

In biological samples, the dominant water NMR signal limits dynamic range, masking solute signals and hindering accurate analysis. We address this with a water suppression technique based on optimal control pulses, enabling high-quality ^{1}H NMR spectra in both high and low-field NMR without specialized equipment.[49] Alternatively, excitation sculpting and pulsed-field gradients offer more effective suppression but require additional hardware.[50] Detailed information is provided in Supporting Information (Section S1).

This work aims to enhance low-field NMR's analytical ability for complex organic mixtures by overcoming challenges like spectral broadening, water suppression, and signal overlapping. Dipolar couplings and limited spectral range in low-field NMR cause broadening and overlap, which complicate chemical structure identification and metabolic assignments.[51,52] Effective water suppression is crucial for accurate quantification. While excitation sculpting and presaturation pulses are viable techniques, they require specialized hardware and may cause incomplete suppression or affect exchangeable protons.[53−55]

THEORY

Optimal Control Theory. Optimal control theory concerns the evolution of quantum systems governed by Hamiltonians that depend on external control fields. A linear perturbation in the Hamiltonian can be used to describe the optimal control scenario.[26−28] Spin system editing is achieved in this work using the Krotov algorithm of optimal control theory, which employs a gradient-based approach that monotonically enhances the objective functional at each iteration.[28] Second-order derivatives are utilized in the algorithm to improve convergence near the optimum.[56] The algorithm of a Krotov-based OC approach is based on the general mathematical formulation of global optimal control methods by Krotov formulation.[28] One of the first practical applications of these methods in Quantum Optimal Control is the work of Zhu and Rabitz.[57] An implementation for NMR applications based on a density operator formulation was carried out in[56] and[54] by Maximov et al. In[45] Vinding et al., the first application of Krotov-based OC pulses for MRI based on a description with Bloch equations. The algorithm used in this work corresponds to the variant of a Krotov-based algorithm described in.[54] It represents a version with stabilized monotonic convergence and additional smoothing of the radiofrequency pulse (RF) pulse shapes.[60,62] Detailed information is provided in Supporting Information (Sections S2 and S3).

Direct Dipolar−Dipolar Coupling. The primary interaction in NMR spectroscopy is the Zeeman interaction, with other interactions such as chemical shielding and dipolar interactions being regarded as perturbations to the Zeeman interaction.[58] Dipolar coupling signifies the direct magnetic interaction between dipoles. The full Hamiltonian for dipolar coupling comprises secular (time-independent) and nonsecular (time-dependent) terms.[59] At high NMR field strengths, the nonsecular part averages to zero, leaving only the secular term. In the case of homonuclear coupling (involving the same isotopes), a flip-flop term exists, leading to transitions between different states of the two coupled spins.

Multiple-Pulse Line Narrowing. Homonuclear dipolar couplings can be eliminated through magic angle spinning (MAS), but in biological systems, MAS can be invasive and potentially harm sample integrity. An alternative approach involves manipulating the nuclear spins themselves using multiple-pulse line narrowing, effectively averaging out the dipolar interactions. This method employs specially designed pulse sequences with precise adjustments in phase, duration, and spacing. One such sequence is the weak amplitude unmodulated homonuclear average (WAHUHA) sequence initially proposed in reference[41,60] for its simplicity and effectiveness. It involves weak RF pulses that are unmodulated where the exact parameters of the sequence, such as pulse duration and spacing, are optimized for the specific sample and type of dipolar coupling. In our case a sequence of four $\pi/2$ pulses were employed. Detailed information is provided in Supporting Information (Sections S4 and S5).

EXPERIMENTAL SECTION

Materials and Chemicals. Phenylalanine (Phe) is an essential α-amino acid with the L-isomer known as (*S*)-2-Amino-3-phenylpropionic acid ($C_6H_5CH_2CH(NH_2)CO_2H$) and a molar mass of 165.192 g/mol. It features a nonpolar, hydrophobic benzyl side chain and is crucial for protein synthesis. Additionally, phenylalanine serves as a precursor for tyrosine, dopamine, norepinephrine, epinephrine, and melanin. It was obtained from Sigma-Aldrich (CAS No. 63−91−2, Germany) and used without further processing.

Taurine (Tau), or 2-aminoethanesulfonic acid ($H_2NCH_2CH_2SO_3H$), has a molar mass of 125.14 g/mol. It was obtained from Sigma-Aldrich (CAS No. 107−35−7, Germany) and used without further processing. Taurine is a nonproteinogenic amino sulfonic acid found in animal tissues, serving as a major component of bile and present in the large intestine, where it contributes up to 0.1% of total human body weight.

Standard agarose (Product No. A8963, CAS Number: 9012−36−6, EC Number: 232−731−8) was used for gel electrophoresis. This agarose is suitable for separating DNA and RNA fragments at concentrations between 0.8 and 2% and is compatible with all common electrophoresis buffer systems.

https://doi.org/10.1021/acs.analchem.3c05226
Anal. Chem. 2025, 97, 1983−1991

It is provided by AppliChem GmbH, and the gel strength is ≥1000 g/cm^2 for 1% gels and ≥2200 g/cm^2 for 1.5% gels, with minimal contamination of DNases, RNases, or proteases.

High-resolution 5 mm borosilicate glass NMR tubes (Boro-600−5−8) were sourced from Deutero GmbH, Kastellaun, Germany. Borosilicate glass capillary tubes with an outer diameter (OD) of 1.7 mm, an inner diameter (ID) of 1.3 mm, and a length of 100 mm were provided by Hilgenberg (Art.-Nr. 2001710, Essen, Germany). Deuterium oxide (D_2O) was obtained from Sigma-Aldrich (CAS No. 7789−20−0, Germany).

Sample Preparation Methods. Agarose gels were prepared to maximize viscosity for dipolar localization in NMR studies. Solutions with concentrations of 0.05, 0.1, 0.15, 2, 2.5, 3, and 4 wt % agarose were tested. Agarose powder was gradually added to D_2O while stirring at 500 rpm on a magnetic stirrer. The mixture was then heated in a microwave at 700 W for 12 s to ensure complete dissolution and homogeneity, taking care to prevent overboiling and maintain the D_2O ratio. A final concentration of 1.5 wt % was selected to achieve maximum dipolar coupling and spectral broadening.

An equimolar mixture of phenylalanine (Phe) and taurine (Tau) was prepared in deuterium oxide (D_2O) with a total volume of 500 μL. Each component was initially prepared at a concentration of 10 mM (0.05 mol per 100 mL). For the final mixture, 200 μL of phenylalanine was combined with 200 μL of taurine. Additionally, 1 mg of 3-(trimethylsilyl)propionic-2,2,3,3-d_4 acid sodium salt ($(CH_3)_3SiCD_2CD_2CO_2Na$) (TSP) was dissolved in 100 mL of D_2O, and 10 μL of this TSP solution was added to the sample.

For low-field NMR samples, Phe-Tau was prepared with phenylalanine and taurine at a concentration of 0.1 mol per 100 mL (10 mM). Subsequently, 10 μL of phenylalanine was mixed with 10 μL of taurine. Additionally, 1 mg of TSP was dissolved in 100 mL of D_2O, resulting in a 10 mL TSP solution. The sample was mixed externally using a microsyringe and then injected into a standard borosilicate 3 mm outer diameter (OD) and 2.8 mm inner diameter (ID) NMR tube.

Spectrometers.

(i) The low-field NMR spectrometer employed in this research was developed using a novel multilayer Halbach magnet, which provides a magnetic field strength of 0.7 T. The B_0 homogeneity achieved was $\Delta B_0/B_0 = 10^{-4}$ within a cylindrical sample volume of 3 mm in diameter and 3 mm in length, achieved without the need for an external shimming system. The integrated on-board probehead was precisely tuned for ^{1}H NMR at a frequency of 29.93 MHz, with the resonance circuit optimized using multiturn tuning and matching capacitors (Voltronics Corp., Salisbury, MD). The NMR detection was facilitated by a solenoidal probehead equipped with an 80 μm diameter copper microcoil, consisting of 12 turns over a length of 1.3 mm. This microcoil was directly fabricated onto a standard NMR tube, which has an inner diameter (ID) of 2.4 mm and an outer diameter (OD) of 3 mm, yielding an inductance of approximately 0.35 μH.[16,61,62] The system was interfaced with the iSpin-NMR 2U instrument from SpinCore Technologies Inc. (console) for the acquisition of low-field ^{1}H NMR spectra.

(ii) High-resolution ^{1}H NMR spectra were acquired using a Bruker AVANCE III NMR spectrometer with a Bruker room temperature probehead operating at 600.13 MHz (B_0 = 14.1 T). HR MAS experiments were performed on the same spectrometer, at the same operating NMR frequency, but with a ^{1}H/^{13}C MAS probe head equipped with a z-gradient coil. TopSpin 3.7 software package was employed for NMR data acquisition, processing, and analysis.[23] Low- and high-field NMR results were plotted and arranged using Orginlab2022. The robust Krotov algorithm was implemented using MATLAB programming language and customized based on the approach proposed by Maximov et al.[28]

Pulse Sequences. The WAHUHA pulse sequence used in the experiments was adapted from previous studies (refs 41 and 60). Detailed information on the pulse timing, phases, and parameters is provided in the Supporting Information (Section S5).

RESULTS AND DISCUSSION

Multisystem Selective Excitation. A homogeneous solution comprising of phenylalanine (Phe) and taurine (Tau) with equal molar concentrations in water was investigated to showcase the utilization of optimal control (OC) pulses for selective excitation and selective excitation. Figure 1 shows the ^{1}H NMR spectra of Phe-Tau mixture in water acquired at low-field (29.93 MHz) and high-field (600.13 MHz) and the resonance frequencies of the signals are summarized in Figure 2. The high-field ^{1}H NMR spectrum of Tau presents two characteristic triplets, positioned at 3.25 and 3.42 ppm, corresponding to the coupled protons (H_3, H_4) and (H_1, H_2) of CH_2-CH_2 taurine backbone, respectively.[63,64]

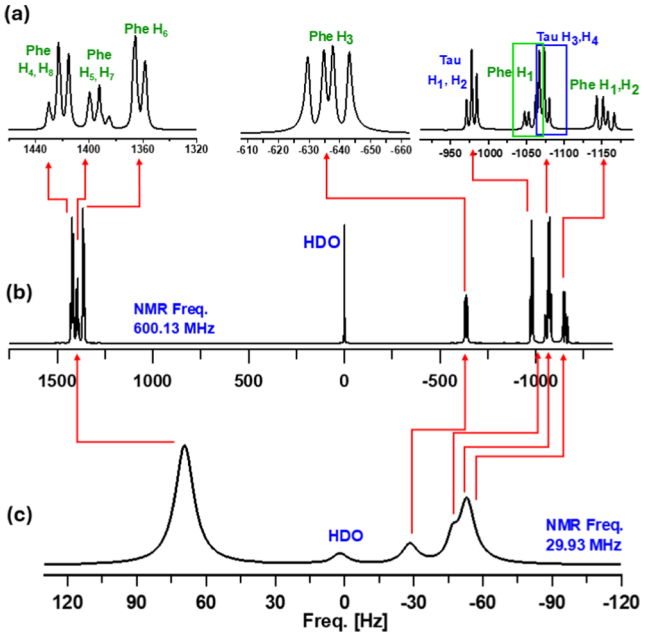

Figure 1. (a) Magnified views of the signals in the 600.13 MHz NMR spectrum reveal the multiplet splitting patterns. The ^{1}H NMR spectra of a homogeneous mixture of Phe and Tau at equal molarities were obtained at (b) 600.13 and (c) 29.93 MHz. High-field and low-field NMR measurements were performed using a Bruker AVANCE III NMR spectrometer and an in-house manufactured spectrometer, respectively.

https://doi.org/10.1021/acs.analchem.3c05226
Anal. Chem. 2025, 97, 1983−1991

Taurine (Tau)			Phenylalanine (Phe)		
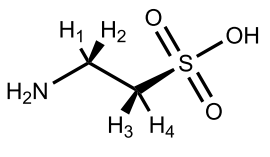			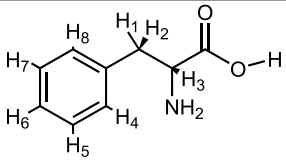		
J-Coupling [Hz]	NMR frequencies [Hz]		Coupling [Hz]	NMR frequencies [Hz]	
	600.13 MHz	29.93 MHz		600.13 MHz	29.93 MHz
J_{13} = 6.74 J_{14} = 6.46 J_{23} = 6.40 J_{24} = 6.79	$\nu_1 = \nu_2$ = -977 $\nu_3 = \nu_4$ = -1070	$\nu_1 = \nu_2$ = -49 $\nu_3 = \nu_4$ = -53	J_{12} = -14.57 J_{13} = 8.01 J_{23} = 5.21 J_{46} = 1.59 J_{68} = 0.97 J_{45} = 7.91 J_{78} = 7.35 J_{67} = 7.53 J_{47} = 0.49 J_{58} = 5.21 J_{57} = 0.99 J_{48} = 1.42	ν_1 = -1057 ν_2 = -1154 ν_3 = -636 $\nu_4 = \nu_8$ = 1359 $\nu_5 = \nu_7$ = 1420 ν_6 = 1390	ν_1 = -53 ν_2 = -58 ν_3 = -32 $\nu_4 = \nu_8$ = 68 $\nu_5 = \nu_7$ = 71 ν_6 = 69

Figure 2. Resonance frequencies and J-couplings of Phe and Tau at 29.93 and 600.13 MHz are visually represented, based on values directly measured and deduced from the experimental NMR spectra. These parameters were determined without additional computational analysis, relying on direct observation of the spectral data.

Notably, these two triplets are unresolved by the low-field NMR (29.93 MHz) and are manifested as broad overlapping signals.[65,66]

The high-field ^{1}H NMR spectrum of Phe-Tau mixture displays eight multiplet signals associated with the coupled protons. The resonance frequencies and J-couplings of Phe and Tau at 29.93 and 600.13 MHz were directly measured and deduced from the experimental NMR spectra (Figure 1). These parameters, including the chemical shifts and splitting patterns, were extracted without additional computational analysis. Based on that and by setting the water signal at 0 Hz, the central resonance peaks of Phe appear at (−1057, −1154, −636, 1359, 1420, 1390 Hz) while for Tau appeared at (−977, −1070 Hz). At low-field NMR, Phe-Tau mixture exhibit three distinct peaks: (i) −52 Hz, which corresponds to the overlapped NMR signals of H_1, H_2, H_3, H_4 in the Tau molecule with the addition of H_1 and H_2 from the Phe molecule, all corresponding in high-field to the frequency range from −1166 to −970 Hz in the high-field spectrum; (ii) −30 Hz, corresponding to the overlapped NMR signals of H_3 in Phe, which corresponds to the frequency range −630 to −643 Hz in the high-filed spectrum; and (iii) 69.5 Hz, corresponding to the overlapped Phe NMR signals of H_4, H_5, H_6, H_7, and H_8 in the Tau-Phe mixture.

Chemical shifts and coupling constants of Phe and Tau were determined using first-order analysis of the 600.13 MHz NMR spectrum (Figure 2). To perform a selective excitation experiment, optimal control (OC) pulses were calculated to selectively excite either Phe or Tau. The strong coupling Hamiltonians for each spin system are described by eqs 1 and 2, corresponding to Phe and Tau, respectively

$$H_{\mathrm{Phe}} = 2\pi \sum_{i=1}^{8} \nu_i^1 I_{zH_i}^1 + 2\pi \sum_{i=1}^{7} \sum_{j=2}^{8} J_{ij}^1 I_{zH_i}^1 \cdot I_{zH_j}^1 \quad (1)$$

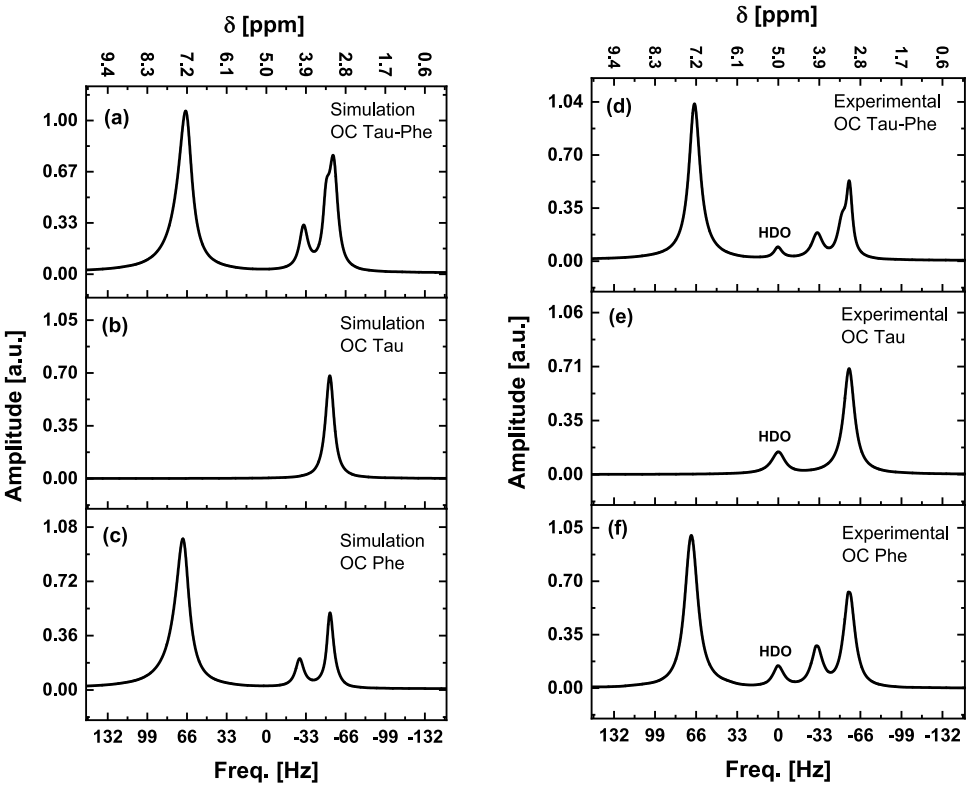

Figure 3. Stack plots of simulated (left) and experimental (right) ^{1}H NMR spectra at 29.93 MHz for a homogeneous Phe-Tau mixture using optimal control pulses. Spectra show: (a, d) excitation of both systems (Phe and Tau) with a hard pulse (HP); (b, e) selective excitation of spin system 1 (Phe); and (c, f) selective excitation of spin system 2 (Tau). The experimental spectra include an HDO signal, absent in simulations since HDO was not modeled, ensuring clarity in experimental comparisons.

https://doi.org/10.1021/acs.analchem.3c05226
Anal. Chem. 2025, 97, 1983−1991

$$H_{\mathrm{Tau}} = 2\pi \sum_{i=1}^{4} \nu_i^2 I_{zH_i}^2 + 2\pi \sum_{i=1}^{2} \sum_{j=3}^{4} J_{ij}^2 I_{zH_i}^2 \cdot I_{zH_j}^2 \quad (2)$$

where the spins ($H_i, i = 2,\cdots,6$) and (H_i, $i = 1,\cdots,4$) are assigned to the Phe and Tau molecules, respectively. Subsequently, three optimal control pulses are applied at 29.93 MHz.

Pulse Optimization. Optimal control pulses often exhibit highly variable, noise-like shapes, which can cause distortions and reduced fidelity if the hardware is not perfectly linear. Therefore, smoothness constraints were applied by filtering the pulses at each iteration and suppressing components far from resonance which produced relatively smooth pulses with experimental performance closely matching theoretical predictions. Additionally, suppressing nonresonant components lowered the total energy and reduced the specific absorption rate. This was demonstrated by the pulse shapes (phase and amplitude) used to selectively excite Phe while not exciting Tau, and vice versa, at an NMR frequency of 600.13 and 29.93 MHz. The detailed pulse calculations, including the significant 2 rad phase jump observed during the evaluation, are provided in Supporting Information (Section S6 and Figure S2).

The initial OC pulse (Figure 3a) acquired at low LF-NMR (29.93 MHz) is tailored to induce excitation in both Phe and Tau molecules, and the resulting ^{1}H NMR spectra, both measured and simulated, are provided. Subsequently, the second and third optimal control pulses are computed to selectively stimulate either the Phe or Tau spectra while concurrently suppressing the other, as depicted in Figure 3b,c, respectively. In experimental validation (Figure 3e) demonstrates the implementation of the pulse designed to excite both Phe and Tau molecules, while Figure 3f,g exhibit the experimental outcomes of employing selective excitation pulses calculated to stimulate either the Phe or Tau spectra while suppressing the other, respectively.

Gaussian pulses (GP) are widely used for selective excitation due to their defined frequency profiles. However, their effectiveness relies on signals being distributed across successive, nonoverlapping frequency ranges throughout the spectrum. In cases where spectral components exhibit significant overlap or appear in nonsuccessive frequency ranges—such as in the Phe-Tau spectrum within 1000−1100 Hz—GP fails to achieve the desired selectivity. This limitation extends to many other systems with overlapping signals distributed across nonsuccessive spectral regions. Nevertheless, to assess the efficacy of both Gaussian pulses and off-resonance irradiation with a carrier frequency (OC) pulse, experiments were conducted using GP with a 1% cutoff, offset at the targeted signal, a maximum power level of 3.16 μW, and a pulse duration of 21.2 ms. Notably, these experiments were conducted solely within the resolved frequency regions of the Phe-Tau spectrum. The excitation and suppression factors for both types of pulses were measured (Supporting Information, Table S1). The results indicate that Gaussian pulses achieved a suppression factor (SF) of 0.03 for the unwanted signal, which is comparable to the performance of Krotov optimized pulses. However, the excitation factor (EF) values for the targeted signals obtained using Gaussian pulses, averaging 0.55 for phenylalanine and 0.53 for taurine, were significantly lower than those achieved with OC pulses, which averaged 0.78 for phenylalanine and 0.77 for taurine. Detailed information is provided in Supporting Information (Sections S7 and S8 and Table S1).

Water Suppression. We present a simple and robust water suppression technique based on an optimal control pulse that enables acquisition of high-quality ^{1}H NMR spectra of metabolites with high- and low-field NMR spectroscopy. The Hamiltonian used for water suppression is provided below

$$H_{\mathrm{water}} = 2\pi \sum_{i=-3}^{3} \nu_i^3 I_{zH_i}^3 (\nu_i^3 = -6, -4, -2, 0, 2, 4, 6 \ \mathrm{Hz};\ i = -3, -2, -1, 0, 1, 2, 3) \quad (3)$$

The Phe-Tau sample was prepared in a solvent containing 10% H_2O and 90% D_2O with a volume of 500 μL.

In Figure 4a, the water signal dominates over the signals from Phe-Tau. However, by employing optimal control pulse

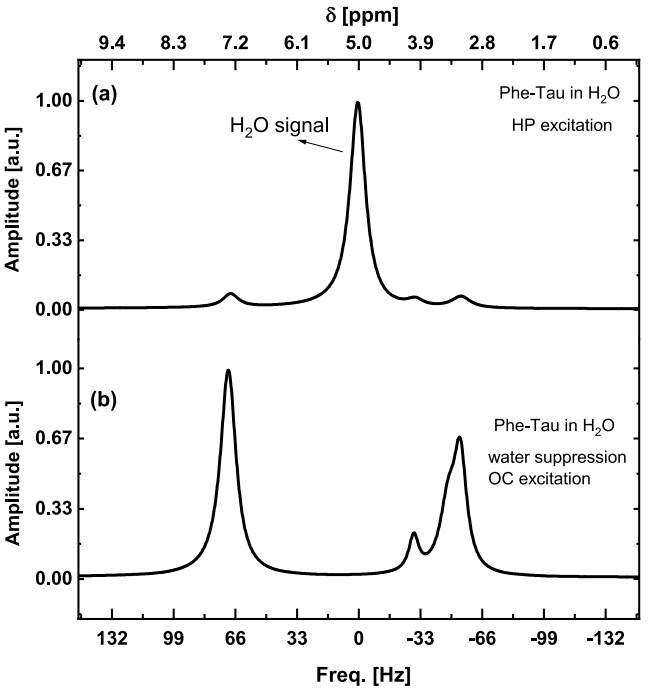

Figure 4. ^{1}H NMR spectra of Phe-Tau in H_2O−D_2O (with 10% D_2O) measured at a frequency of 29.93 MHz. The NMR spectra were obtained using two excitation methods: (a) conventional hard pulse excitation and (b) optimized control pulse excitation, where the water signal was selectively suppressed, and only the Phe and Tau signals were excited.

excitation, including water-suppressing OC pulses (Figure 4b), effective water suppression was achieved without increasing the experimental duration. Furthermore, the amplitude and area under the Phe-Tau signal after water suppression with optimal control are comparable to those in the spectrum shown in Figure 3, where the Phe-Tau analyte was measured in D_2O.

Dipolar Decoupling: WAHUHA. Agarose gel (1.5 wt %) was selected as the material, serving as an intermediate between solid-state and liquid-state NMR, to investigate the performance of the WAHUHA sequence. The viscosity of the agarose gel was adjusted to achieve an approximate line width of 20 Hz, making it a suitable approximation for biological tissue.

The implementation of the WAHUHA sequence for acquiring Phe-Tau NMR spectra at a frequency of 29.93 MHz resulted in a significant reduction in the line width at half-maximum, decreasing from 20 to 15 Hz (Figure 5a,b).

https://doi.org/10.1021/acs.analchem.3c05226
Anal. Chem. 2025, 97, 1983−1991

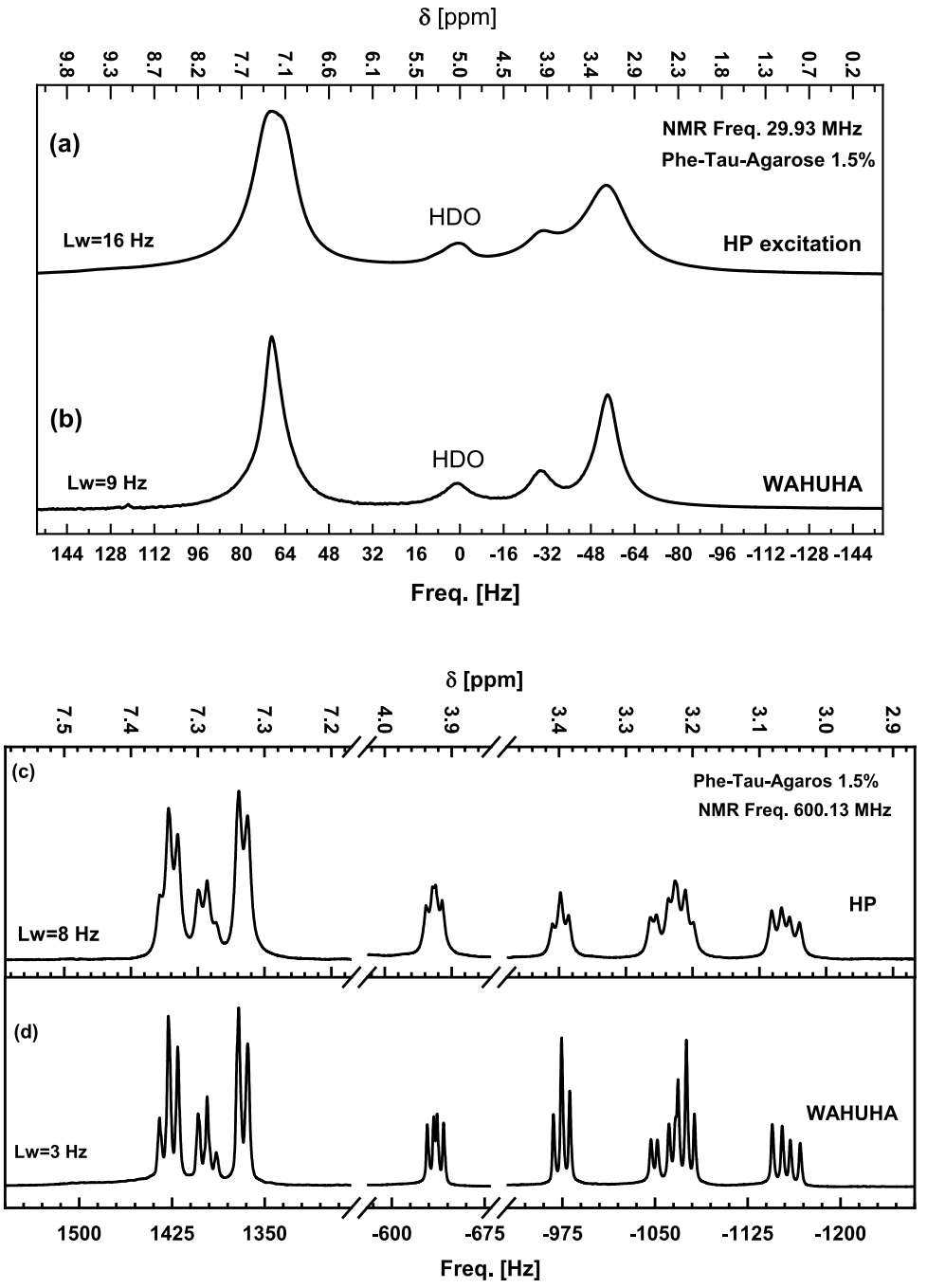

Figure 5. Comparison of ^{1}H NMR spectra for Phe-Tau in D_2O and agarose gel (1.5 wt %) measured at NMR frequencies of 29.93 and 600.13 MHz, respectively. The spectrum in (a) corresponds to standard hard pulse excitation, while (b) shows the spectrum acquired using the multiple-pulse WAHUHA sequence, which effectively eliminates homonuclear dipolar coupling. The spectrum in (c) represents the Phe-Tau sample in D_2O, and (d) demonstrates the Phe-Tau sample in agarose gel using the same WAHUHA sequence at high magnetic field.

Furthermore, applying the WAHUHA sequence to the Phe-Tau sample in combination with agarose gel at high-field NMR (600.13 MHz) reduced the average line width from 8 to 3 Hz (as demonstrated in Figure 5c,d). In general, multiple-pulse sequences such as WAHUHA not only average the dipolar Hamiltonian but also influence other Hamiltonians, including chemical shift anisotropies (CSA), to an extent determined by the specific sequence. Notably, the WAHUHA sequence scales CSA by a factor of $1/\sqrt{3}$. To account for this scaling effect, the chemical shifts were corrected post-WAHUHA application using the internal reference compound TSP.

At low field, the line width of Phe-Tau in D_2O without agarose gel was approximately 12 Hz (Figure 3). Using the WAHUHA sequence eliminated up to 85% of dipolar coupling at both low and high fields. High-resolution magic angle spinning (HRMAS) measurements (Figure 6c,d) at spinning rates of 2000 and 3000 rpm achieved an average line width reduction of ∼5 Hz compared to static measurements. Notably, this reduction matched the improvement observed with the WAHUHA sequence.

https://doi.org/10.1021/acs.analchem.3c05226
Anal. Chem. 2025, 97, 1983−1991

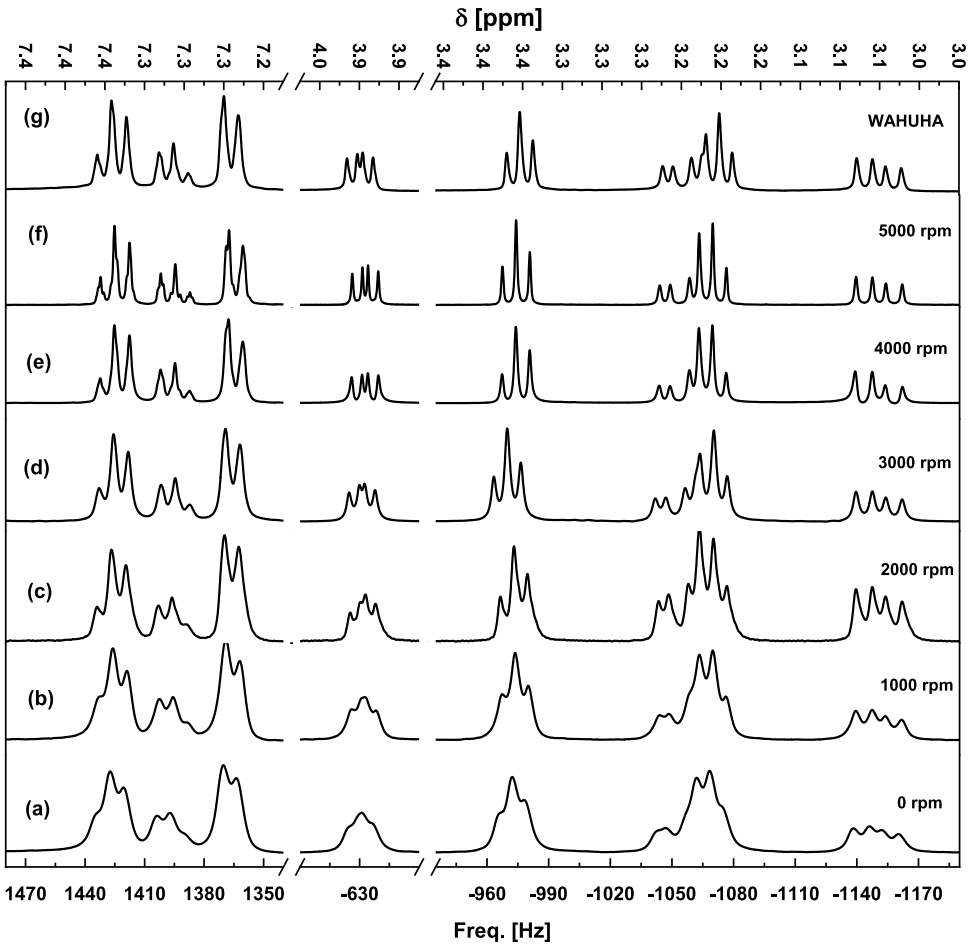

Figure 6. Comparison of ^{1}H NMR high-resolution magic angle spinning (HRMAS) spectra of Phe-Tau in D_2O and agarose gel (1.5 wt %) acquired at a NMR frequency of 600.13 MHz. The spectra were measured at different spinning rates: (a) 0, (b) 1000, (c) 2000, (d) 3000, (e) 4000, and (f) 5000 rpm. (g) The effectiveness of the multiple-pulse WAHUHA sequence in eliminating homonuclear dipolar coupling is comparable to the HRMAS spectra obtained at spinning rates between 2000 and 3000 rpm.

CONCLUSIONS

This study tackles the challenges of low-field NMR by using optimal control (OC) pulses. These specialized pulses allow researchers to selectively excite specific molecules—like metabolites in complex mixtures—at both low-field (29.93 MHz) and high-field (600.13 MHz) NMR. Using the Krotov algorithm to fine-tune the pulses, the team was able to isolate phenylalanine (Phe) or taurine (Tau) from a mixture, even when their signals overlapped significantly in the 1000−1100 Hz range. The method allowed precise targeting of the desired signals while minimizing interference from others. Additionally, the study used a multiple-pulse WAHUHA sequence combined with 1.5% agarose, which reduced homonuclear dipolar coupling by about 85% across both low and high-field NMR, comparable to the performance of HRMAS spinning rates at 2000−3000 rpm. Water suppression was also effectively handled by treating water molecules as a separate system in the Hamiltonian of the mixture. Overall, the integration of OC pulses, water suppression, and the WAHUHA sequence shows great promise for enhancing low-field NMR as a programmable detector.

ASSOCIATED CONTENT

Supporting Information

The Supporting Information is available free of charge at https://pubs.acs.org/doi/10.1021/acs.analchem.3c05226.

Challenges in NMR water suppression; optimal control theory for pulse design; Krotov-Based optimization algorithm; dipolar coupling in NMR; multiple-pulse NMR line narrowing. WAHUHA; optimal control pulse optimization, and comparative analysis of water suppression techniques. schematic of the multiple-pulse WAHUHA sequence implemented in Bruker's AU programming language (Figure S1); displaying pulse shapes for selective excitation of Phe and Tau in low-field and high-field NMR (Figure S2); comparative 1H-NMR spectra showing various water suppression techniques and their impact on spectral quality (Figure S3); detailing the efficiency and suppression factors (EF and SF) for Gaussian and optimal control pulses in water suppression (Table S1) (PDF)

AUTHOR INFORMATION

Corresponding Authors

Ahmed Bahti − *Experimental Physics III, TU Dortmund University, Dortmund 44227, Germany; Leibniz-Institut für Analytische Wissenschaften - ISAS - e.V., Dortmund 44139,*

https://doi.org/10.1021/acs.analchem.3c05226
Anal. Chem. 2025, 97, 1983−1991

Germany; orcid.org/0000-0003-3256-791X; Email: ahmed.bahti@tu-dortmund.de

Dieter Suter − *Experimental Physics III, TU Dortmund University, Dortmund 44227, Germany*; Email: dieter.suter@tu-dortmund.de

Authors

Ahmad Telfah − *Cell Therapy Center, The University of Jordan, Amman 11942, Jordan; Department of Physics, University of Nebraska at Omaha, Omaha, Nebraska 68182, United States*; orcid.org/0000-0003-1478-8620

Roland Hergenröder − *Leibniz-Institut für Analytische Wissenschaften - ISAS - e.V., Dortmund 44139, Germany*

Complete contact information is available at: https://pubs.acs.org/10.1021/acs.analchem.3c05226

Author Contributions

A.B., A.T., R.H., and D.S.: Conceptualization. A.B. and A.T: Methodology. A.B. and A.T.: Software. A.B., A.T., R.H. and D.S.: Validation. A.B., A.T. and R.H.: Formal analysis. A.B. and A.T.: Investigation. A.B., A.T. and R.H.: Resources. A.B., A.T. and R.H.: Data curation. A.B. and A.T.: Writing—original draft preparation. A.B., A.T., R.H. and D.S.: Writing—review and editing. A.B., A.T., R.H.: Visualization. A.T., R.H. and D.S.: Supervision. All authors have read and agreed to the published version of the manuscript.

Notes

The authors declare no competing financial interest.

■ ACKNOWLEDGMENTS

The scientific support by the Ministerium für Innovation, Wissenschaft und Forschung des Landes Nordrhein−Westfalen, the Senatsverwaltung für Wirtschaft, Technologie und Forschung des Landes Berlin, and the Bundesministerium für Bildung und Forschung is gratefully acknowledged.

■ REFERENCES

(1) Blümich, B. *J. Magn. Reson.* **2019**, *306*, 27−35.
(2) Blümler, P.; Casanova, F. Hardware Developments: Halbach Magnet Arrays. In *Mobile NMR and MRI: Developments and Applications* 2015; pp 133−157.
(3) Anders, J.; Lips, K. *J. Magn. Reson.* **2019**, *306*, 118−123.
(4) Grootveld, M.; Percival, B.; Gibson, M.; et al. *Anal. Chim. Acta* **2019**, *1067*, 11−30.
(5) Luy, B. *Angew. Chem., Int. Ed.* **2011**, *50* (2), 354−356.
(6) Antonides, L. H.; Brignall, R. M.; Costello, A.; et al. *Acs Omega* **2019**, *4* (4), 7103−7112.
(7) Assemat, G.; Gouilleux, B.; Bouillaud, D.; et al. *J. Pharm. Biomed. Anal.* **2018**, *160*, 268−275.
(8) Duffy, J.; Urbas, A.; Niemitz, M.; Lippa, K.; Marginean, I. *Anal. Chim. Acta* **2019**, *1049*, 161−169.
(9) Fallaise, D.; Tweedie, H. B.; Konzuk, J.; Cheyne, C.; Mack, E. E.; Longstaffe, J. G. *Magn. Reson. Chem.* **2019**, *57* (2−3), 93−100.
(10) Leutzsch, M.; Sederman, A. J.; Gladden, L. F.; Mantle, M. D. *Magn. Reson. Imaging* **2019**, *56*, 138−143.
(11) Gołowicz, D.; Kazimierczuk, K.; Urbańczyk, M.; Ratajczyk, T. *ChemistryOpen* **2019**, *8* (2), 196−200.
(12) Gouilleux, B.; Christensen, N. V.; Malmos, K. G.; Vosegaard, T. *Anal. Chem.* **2019**, *91* (4), 3035−3042.
(13) Sørensen, M. K.; Balsgart, N. M.; Jensen, O.; Nielsen, N. C.; Vosegaard, T. *ChemPhysChem* **2018**, *19* (22), 2985−2988.
(14) Lindon, J. C.; Tranter, G. E.; Koppenaal, D. *Encyclopedia of Spectroscopy and Spectrometry*; Academic Press, 2016.
(15) Webb, G. A. *Annu. Rep. Prog. Chem., Sect. C:Phys. Chem.* **1995**, *80*, 39−85.
(16) Telfah, A.; Bahti, A.; Kaufmann, K.; Ebel, E.; Hergenröder, R.; Suter, D. *Sci. Rep.* **2023**, *13* (1), No. 21092.
(17) Dalitz, F.; Cudaj, M.; Maiwald, M.; Guthausen, G. *Prog. Nucl. Magn. Reson. Spectrosc.* **2012**, *60*, 52−70.
(18) Rudszuck, T.; Förster, E.; Nirschl, H.; Guthausen, G. *Magn. Reson. Chem.* **2019**, *57* (10), 777−793.
(19) Aydin, E.; Makinwa, K. A. *A Low-Field Portable Nuclear Magnetic Resonance (NMR) Microfluidic Flowmeter*; 21st International Conference on Solid-State Sensors, Actuators and Microsystems (Transducers); IEEE, 2021; pp 1020−1023.
(20) Gong, Q.; Gordji-Nejad, A.; Blümich, B.; Appelt, S. *Anal. Chem.* **2010**, *82* (17), 7078−7082.
(21) Castaing-Cordier, T.; Bouillaud, D.; Bowyer, P.; Gonçalves, O.; Giraudeau, P.; Farjon, J. *ChemPhysChem* **2019**, *20* (5), 736−744.
(22) McCarney, E. R.; Dykstra, R.; Galvosas, P. *Magn. Reson. Imaging* **2019**, *56*, 103−109.
(23) Chinthalapalli, S.; Bornet, A.; Segawa, T. F.; Sarkar, R.; Jannin, S.; Bodenhausen, G. *Phys. Rev. Lett.* **2012**, *109* (4), No. 047602.
(24) Skinner, T. E.; Reiss, T. O.; Luy, B.; Khaneja, N.; Glaser, S. J. *J. Magn. Reson.* **2003**, *163* (1), 8−15.
(25) Skinner, T. E.; Reiss, T. O.; Luy, B.; Khaneja, N.; Glaser, S. J. *J. Magn. Reson.* **2005**, *172* (1), 17−23.
(26) Maday, Y.; Salomon, J.; Turinici, G. *Numer. Math.* **2006**, *103* (2), 323−338.
(27) Maximov, I. I.; Tošner, Z.; Nielsen, N. C. *J. Chem. Phys.* **2008**, *128* (18), No. 184505.
(28) Maximov, I. I.; Salomon, J.; Turinici, G.; Nielsen, N. C. *J. Chem. Phys.* **2010**, *132* (8), No. 084107.
(29) Holbach, M.; Lambert, J.; Suter, D. *J. Magn. Reson.* **2014**, *243*, 8−16.
(30) Holbach, M.; Lambert, J.; Johst, S.; Ladd, M. E.; Suter, D. *J. Magn. Reson.* **2015**, *255*, 34−38.
(31) Khaneja, N.; Reiss, T.; Kehlet, C.; Schulte-Herbrüggen, T.; Glaser, S. J. *J. Magn. Reson.* **2005**, *172* (2), 296−305.
(32) Gowda, G. N.; Raftery, D. *NMR-Based Metabolomics: Methods and Protocols*; Springer, 2019.
(33) Alexandri, E.; Ahmed, R.; Siddiqui, H.; Choudhary, M. I.; Tsiafoulis, C. G.; Gerothanassis, I. P. *Molecules* **2017**, *22* (10), No. 1663.
(34) Anisimov, O.; Nikitaev, A.; Zamaraev, K. I.; Molin, Y. N. *Theor. Exp. Chem.* **1974**, *7*, 556−559.
(35) El Nokab, M. E. H.; van der Wel, P. C. *Carbohydr. Polym.* **2020**, *240*, No. 116276.
(36) Shapiro, M. J.; Gounarides, J. S. *Biotechnol. Bioeng.* **2000**, *71* (2), 130−148.
(37) Wind, R. A.; Hu, J. Z. *Prog. Nucl. Magn. Reson. Spectrosc.* **2006**, *49*, 207−259, DOI: 10.1016/j.pnmrs.2006.05.003.
(38) Polenova, T.; Gupta, R.; Goldbourt, A. *Anal. Chem.* **2015**, *87*, 5458−5469, DOI: 10.1021/ac504288u.
(39) Calucci, L.; Veracini, C. A. Liquid Crystals and Liquid Crystal Solutions Studied by NMR. In *Encyclopedia of Spectroscopy and Spectrometry*; Academic Press, 1999; pp 1179−1186.
(40) Alam, T. M.; Jenkins, J. E.HR-MAS NMR Spectroscopy in Material Science. In *Advanced Aspects of Spectroscopy*, 2012; Vol. *10*, p 279.
(41) Waugh, J. S.; Huber, L.; Haeberlen, U. *Phys. Rev. Lett.* **1968**, *20* (5), No. 180.
(42) Renault, M.; Shintu, L.; Piotto, M.; Caldarelli, S. *Sci. Rep.* **2013**, *3* (1), No. 3349.
(43) Gogiashvili, H. *Metabolites* **2019**, *9*, No. 19, DOI: 10.3390/metabo9020019.
(44) Huang, Y.; Zhang, Z.; Chen, H.; Feng, J.; Cai, S.; Chen, Z. *Sci. Rep.* **2015**, *5* (1), No. 8390.
(45) Paruzzo, F. M.; Emsley, L. *J. Magn. Reson.* **2019**, *309*, No. 106598.
(46) Zhang, R.; Mroue, K. H.; Sun, P.; Ramamoorthy, A. High-Resolution Proton NMR Spectroscopy of Polymers and Biological Solids. In *Modern Magnetic Resonance*; Springer, 2018; Vol. *2*, pp 1−16.

(47) Waugh, J. S.; Huber, L. M.; Haeberlen, U. *Phys. Rev. Lett.* **1968**, *20* (5), No. 180.
(48) Choi, J.; Zhou, H.; Knowles, H. S.; Landig, R.; Choi, S.; Lukin, M. D. *Phys. Rev. X* **2020**, *10* (3), No. 031002.
(49) Bothwell, J. H. F.; Griffin, J. L. *Biol. Rev.* **2011**, *86* (2), 493−510.
(50) Hwang, T.-L.; Shaka, A. *J. Magn. Reson., Ser. A* **1995**, *112* (2), 275−279.
(51) Slichter, C. P. *Principles of magnetic resonance*. Springer Science & Business Media, 2013.
(52) Dybowski, C. Zeeman Interaction in Nuclear Magnetic Resonance. In *Encyclopedia of Analytical Chemistry: Applications, Theory and Instrumentation*; Wiley, 2006.
(53) Canton, M.; Roe, R.; Poigny, S.; Renault, J.-H.; Nuzillard, J.-M. *Magn. Reson.* **2020**, *1* (2), 155−164.
(54) Botana, L. M. *Seafood and Freshwater Toxins: Pharmacology, Physiology, and Detection*, 3rd ed.; CRC Press, 2014.
(55) Altieri, A. S.; Byrd, R. A. *J. Magn. Reson., Ser. B* **1995**, *107* (3), 260−266.
(56) Machnes, S.; Sander, U.; Glaser, S. J.; et al. *Phys. Rev. A* **2011**, *84* (2), No. 022305.
(57) Zhu, W.; Rabitz, H. *J. Chem. Phys.* **1998**, *109* (2), 385−391.
(58) Ramsey, N. F.; Purcell, E. *Phys. Rev.* **1952**, *85* (1), No. 143.
(59) Sauerwein, A. C. Estimations of Dipolar Couplings in Multiple-Spin Systems by Solid State NMR; PhD Thesis; University of Southampton, 2010.
(60) Miller, J. B.; Cory, D.; Garroway, A. *Rev. Prog. Quant. Nondestr. Eval.* **1992**, 649−654.
(61) Gupta, M.; Safvan, C.; Singh, K.; Lobiyal, D.; Yadav, P.; Singh, S. *IEEE Sens. J.* **2019**, *19* (7), 2500−2508.
(62) Bahti, A.; Telfah, A.; Lambert, J.; Hergenröder, R.; Suter, D. *J. Magn. Reson.* **2021**, *328*, No. 106993.
(63) Simoyi, R. H.; Streete, K.; Mundoma, C.; Olojo, R. *S. Afr. J. Chem.* **2002**, *55*, 136−143.
(64) Wishart, D. S.; Guo, A.; Oler, E.; et al. *Nucleic Acids Res.* **2022**, *50* (D1), D622−D631.
(65) Meriles, C. A.; Sakellariou, D.; Heise, H.; Moulé, A. J.; Pines, A. *Science* **2001**, *293* (5527), 82−85.
(66) Perlo, J.; Demas, V.; Casanova, F.; et al. *Science* **2005**, *308* (5726), No. 1279.

https://doi.org/10.1021/acs.analchem.3c05226
Anal. Chem. 2025, 97, 1983−1991

Supporting Information

NMR Spectral Editing, Water Suppression and Dipolar Decoupling in Low-Field NMR Spectroscopy using Optimal Control Pulses and Multiple-Pulse Sequence

Ahmed Bahti[a, b*], *Ahmad Telfah*[c,d], *Roland Hergenröder*[b], *Dieter Suter*[a,**]

[a] *Experimental Physics III, TU Dortmund University, 44227 Dortmund, Germany*
[b] *Leibniz-Institut für Analytische Wissenschaften - ISAS - e.V., 44139 Dortmund, Germany*
[c] *Cell Therapy Center, The University of Jordan, 11942, Amman, Jordan*
[d] *Department of Physics, University of Nebraska at Omaha, Omaha NE-68182, USA*

* *e-mail: ahmed.bahti@tu-dortmund.de*
** *e-mail: dieter.suter@tu-dortmund.de*

Table of content

Page	Section	Title
S2	S1.	Challenges in NMR water suppression
S3	S2.	Optimal control theory
S3	S3.	Krotov-based algorithm
S5	S4.	Dipolar coupling
S6	S5.	Multiple-pulse NMR line narrowing
S8	S6.	Optimal Control Pulse Optimization
S9	S7.	Comparative Analysis of Water Suppression Techniques in Low-Field NMR
S10	S8.	Excitation and Suppression Factors (EF and SF)
S7	Figure S1	Schematic representation of the multiple-pulse WAHUHA sequence implemented using the AU programming language of Bruker.
S9	Figure S2	Pulse shapes (amplitude and phase) of the optimal controlled pulses to selectively excite Phe and Tau molecules at **(a)** low-field NMR (29.93 MHz) and **(b)** high-field NMR (600.13 MHz).
S10	Figure S3	^{1}H-NMR spectra of Phe-Tau in H_2O-D_2O (with 10% D_2O) recorded at a frequency of 29.93 MHz. The NMR spectra were acquired using **(a)** hard pulse excitation, **(b)** hard pulse excitation with included water suppression, and **(c)** hard pulse excitation of the same Phe-Tau system, dissolved in pure D_2O to eliminate the water signal for comparative analysis.
S11	Table S1	EF and SF for Gaussian and OC Pulses.

S1. Challenges in NMR water suppression

In biological samples, suppressing the dominant water signal is essential to prevent it from masking solute signals and to enable accurate quantitative analysis [1]. Ideally, after water suppression, NMR spectra should exhibit a flat baseline around the water resonance, with frequencies both lower and higher than the water resonance unaffected. Additionally, the phase of NMR signals should be adjustable through first- and second-order phase corrections. Various techniques have been developed for water suppression, each with distinct advantages and limitations:

Pre-Saturation Methods. These involve applying RF pulses to selectively suppress the water signal. However, pre-saturation often leads to incomplete suppression and introduces delays between successive measurements, which can be particularly challenging for in-situ NMR studies requiring fast data acquisition. Additionally, pre-saturation can transfer its effects to exchangeable protons, complicating their quantification [2-4]. Another limitation is partial saturation near the resonance, which can cause inaccuracies in quantification, as seen with the anomeric protons of α- and β-glucose at 5.23 ppm and 4.67 ppm, respectively.

Pulsed Gradients and Excitation Sculpting. Excitation sculpting uses pulsed field gradients and highly selective pulse sequences for water suppression. While effective, it requires specialized hardware, making it less accessible for routine applications [5].

To address these limitations, we implemented a non-invasive and straightforward water suppression technique based on optimal control pulses. This approach enables the acquisition of high-quality ^{1}H-NMR spectra of metabolites in both high- and low-field NMR spectroscopy without requiring specialized pulse sequences or equipment. This technique eliminates the need for delays between measurements, offering a robust solution for rapid data acquisition.

In addition to water suppression, advanced techniques such as pure shift NMR, diffusion-ordered spectroscopy (DOSY), and long-lived-coherence correlation spectroscopy (LLC-COSY) have been developed to tackle signal overlap and spectral broadening. However, these methods often require specialized equipment and may reduce the signal-to-noise ratio (SNR), limiting their applicability, particularly in low-field NMR experiments [6, 7]. Water suppression is critical in low-field NMR, where dipolar couplings and limited spectral ranges cause signal broadening and overlap. Effective suppression improves spectral resolution, sensitivity, and the accuracy of chemical and metabolic analysis in complex biological systems [8-10].

S2. Optimal control theory

Optimal Control (OC) theory, originally developed for optimizing complex dynamic systems, is a powerful tool for designing advanced pulse sequences in NMR spectroscopy [11, 12]. OC enhances coherence transfer efficiency between spin states and enables precise shaping of the nuclear spin Hamiltonian, leading to novel, high-performance pulse sequences applicable in both liquid- and solid-state NMR [13, 14]. OC techniques optimize r.f. pulse shapes for two primary objectives: maximizing coherence transfer from an initial spin state (ρ_0) to a target state (ρ_D) or achieving a desired effective Hamiltonian. The Liouville-von Neumann equation governs this process, describing spin system evolution via the density operator $\rho(t)$:

$$\frac{d\rho(t)}{dt} = -i[H(t), \rho(t)], \tag{1}$$

with the nuclear spin Hamiltonian $H(t)$ and the density matrix $\rho(t)$.

$$\frac{dU(t)}{dt} = -iH(t)U(t), \tag{2}$$

where $U(t)$ is the unitary propagator, the nuclear spin Hamiltonian is given by

$$H(t) = H_0 + \sum_k \omega_k I_k, \tag{3}$$

where H_0 is the system Hamiltonian describes the internal spin interactions and $\sum_k \omega_k I_k$ is the control Hamiltonian, respectively, resulting in

$$\frac{d}{dt}U_n(t) = -i\left[H_0 + \sum_k \omega_{k,n} I_k\right]U_n(t). \tag{4}$$

The Liouville equation is introduced as a constraint using a complex valued operator $B(t)$ (back propagation function) as a Lagrange multiplier. Then, the necessary conditions for its maximum are found by variational principles. The optimal solution of the problem should satisfy

$$\frac{d}{dt}B(t) = -iH(t)B(t) \tag{5}$$

$$B(T) = \frac{\partial \emptyset_j}{\partial U(T)} \tag{6}$$

$$\omega_k(t) = \frac{1}{\lambda}\mathrm{Im}\{\mathrm{Tr}[B^\dagger(t) I_k U(t)]\}. \tag{7}$$

These equations describe stationary points of the functional, but additional steps are needed to confirm whether these represent global optima.

S3. Krotov-based algorithm

The Krotov algorithm is based on the optimization of a function of the type

$$J_j(\omega_k) = \emptyset_j - \lambda \int_0^T \sum_k \omega_k^2(t)dt, \tag{2.32}$$

where $\emptyset_j$ is the efficiency (fidelity) to be maximized and the second term penalties the deposited power scaled with the weighting factor λ, and T is the duration of the pulse.

$$\emptyset_j = |\mathrm{Tr}(U'_D U)|^2. \tag{9}$$

The functional $J_j(\omega_k)$ must be optimized under the constraint of the Liouville Equation 1

As $J_j(\omega_k)$ has to remain real valued, the complex conjugate of the Lagrange multiplier term has to be added as well,

$$J_j(\omega_k) = \emptyset_j - \lambda \int_0^T \sum_k \omega_k^2(t)dt - \int_0^T Tr\left\{ B^+(t)\left[\frac{d}{dt}U(t) + iH(t)U(t)\right]\right\}dt$$
$$- \int_0^T Tr\left\{\left[\tfrac{d}{dt}U^+(t) - iU^+(t)H(t)\right]B(t)\right\}dt. \tag{10}$$

The optimization requires derivatives of the functional $J_j(\omega_k)$ with respect to the control parameters to be zero at a stationary point, resulting in the following equations:

$$\tfrac{d}{dt}B(t) = -iH(t)\,B(t) \tag{11}$$

$$B(t) = \tfrac{\partial \emptyset_j}{\partial U(T)} \tag{12}$$

$$\omega_k(t) = \tfrac{1}{\lambda} ImTr\{[B^+(t)\, I_k\, U(t)]\}. \tag{13}$$

As the functional $J_j(\omega_k)$ is supposed to increase with each iteration n, the following expression must be positive,

$$\emptyset_{n+1} - \phi_n - \lambda \sum_k \int_0^T \left[\omega_{k,n+1}^2(t) - \omega_{k,n}^2(t)\right]dt. \tag{14}$$

Importing the stationary point conditions and evolving the propagators using the second order Strang method [15], one arrives at

$$f_j(\omega'_j) = 2Re\left[Tr\left\{\left(\exp\left(i\Delta t \sum_k \omega_{k,j-1}H_k\right)\exp\left(-i\Delta t \sum_k \omega'_{k,j-1}H_k\right) - E\right)AU'_{j-1}B_{j-1}A^+\right\}\right]$$
$$- \Delta t\lambda \sum_k (\omega'_{k,j-1} - \omega_{k,j-1})(\omega'_{k,j-1} + \omega_{k,j-1}), \tag{15}$$

which must be optimized to keep the functional difference positive. Here the primed and unprimed variables refer to iteration number $n+1$ and n, respectively, j denotes the number of the time step of length Δt, $A = e^{-i0.5\Delta t H_0}$ and E is the identity operator. The minimization of $-f_j(\omega'_j)$ is started with an appropriate initial guess for the ω_j, using a quasi-Newton optimizer. To take static and r.f. field inhomogeneity into account, the final cost term $\emptyset$ of the optimal control functional can be replaced by a sum $\sum_j \phi_j$ over a range of conditions,

$$J(\omega_k) = \sum_i |\mathrm{Tr}(U'_D U_i)|^2 - \lambda \int_0^T \sum_k \omega_k^2(t)dt, \tag{16}$$

where U_D is the desired propagator, U_D' being the adjoint of U_D and the U_i are the propagators corresponding to Hamiltonians (H_i) which characterize the transformation properties of the robust pulse. The H_i are derived as follows: The static field inhomogeneity (SFI) is considered by the introduction of additional chemical shift terms with higher and/or lower resonance frequencies in the system's Hamiltonian, while the control Hamiltonian is left unchanged. On the other hand, to consider radio-frequency field inhomogeneity (RFI) pre-factors for the control amplitudes are introduced, while the system Hamiltonians are left unchanged. The Hamiltonians H_i are then used for the forward propagation of the U_i and the backward propagation of the B_i in every step of the iteration. The term $AU'_{j-1}B_{j-1}A^{+}$in Equation (9) for the update of the control amplitudes (ω_k) has to be replaced by a sum $\sum_i A_i U'_{i,j-1}B_{i,j-1}A_i^{+}$ over all SFI and RFI conditions, yielding,

$$f_i(\omega'_j) = 2Re\left[Tr\left\{(\exp(i\Delta t\sum_k \omega_{k,j-1}H_k)\exp(-i\Delta t\sum_k \omega'_{k,j-1}H_k) - E)\sum_i A_i\, U'_{i,j-1}B_{i,j-1}A_i^{+}\right\}\right] - \Delta t\lambda\sum_k(\omega'_{k,j-1} - \omega_{k,j-1})(\omega'_{k,j-1} + \omega_{k,j-1}). \quad (17)$$

To reduce the exponential complexity of the algorithm, which poses a heavy computational burden on calculations of pulses for more than 8 spins, the spin system of each chemical compound (I) is considered a system with a distinct system Hamiltonian ($H_{0,1}$) a distinct propagator ($U_{D,I}$), to be synthesized and a set of SFI/RFI propagators ($U_{i,I}$) and back propagators $B_{i,I}$. The sums over all SFI/RFI conditions in Equations (18) and (19) then read,

$$J = \sum_i |\mathrm{Tr}(U'_{D,I}U_{i,I})|^2 - \lambda\int_0^T\sum_k \omega_k^2(t)dt\,. \quad (18)$$

And

$$f_i(\omega'_j) = 2Re\left[Tr\left\{(\exp(i\Delta t\sum_k \omega_{k,j-1}H_k)\exp(-i\Delta t\sum_k \omega'_{k,j-1}H_k - E)\sum_i A_{i,I}\, U'_{i,j-1,I}B_{i,j-1,I}A_{i,I}^{+}\right\}\right] - \Delta t\lambda\sum_k(\omega'_{k,j-1} - \omega_{k,j-1})(\omega'_{k,j-1} + \omega_{k,j-1}). \quad 19)$$

S4. Dipolar coupling

Dipolar coupling represents the direct magnetic interaction between dipoles and is described by a Hamiltonian that includes secular terms, which survive time averaging in the rotating frame, and non-secular terms, which oscillate rapidly and average out [16]. For homonuclear coupling (same isotopes), flip-flop terms cause transitions between states of coupled spins, leading to peak splitting or multiplet

formation. This effect can be mitigated by increasing the external field strength or the magic angle spinning (MAS) rate

The dipolar Hamiltonian for identical spins is given by eq. (20) [17, 18]:

$$H^{dip} = \sum_{i>j} \omega_{ij}^{D,dip} \; \mathrm{D}_{00}^{2}(\Omega_{ij}^{PL,dip}) \left(2I_{iz}I_{jz} - \frac{1}{2}(I_{i+}I_{j-} + I_{i-}I_{j+})\right), \tag{20}$$

in which the sum over all pairs of nuclei, $\omega_{ij}^{D,dip} = -\mu_0\gamma_I^2\hbar/4\pi r_{ij}^3$ is the homonuclear coupling, in which r_{ij} is the internuclear distance, and $\Omega_{ij}^{PL,dip}$ is the set of Euler angles for the transformation from the principal axis system of the dipolar interaction tensor to the laboratory frame. The term $\frac{1}{2}(I_{i+}I_{j-} + I_{i-}I_{j+})$ represents spin-flip interactions for spin i, accounting for non-secular terms in the dipolar Hamiltonian. The I_{i+}, I_{j+} and I_{i-}, I_{j-} are the spin raising and lowering operators for spin i and j respectively.

The Zeeman Hamiltonian is defined as:

$$H_Z = -\gamma\hbar B_0\left(I_{z_1} + I_{z_2}\right), \tag{21}$$

where B_0 represents the static field. The Hamiltonian of the local field (B_{loc}) created by spin 1 at the location of spin 2 can be approximated as:

$$B_{loc} \cong \frac{\gamma\hbar}{r^3} m_1, \tag{22}$$

where m_1 is $\pm 1/2$. In the case of nuclei, $\gamma_n, r = a \sim 3A$, and the magnitude of the local field is on the order of $\sim 10^{-4}$ T . The line broadening $\Delta\omega$ resulting from the dipolar coupling with the surrounding spin bath can be expressed as:

$$\frac{\Delta\omega}{\omega} = \frac{B_{loc}}{B_0} \cong 10^{-4}. \tag{23}$$

S5. Multiple-pulse NMR line narrowing

The J-coupling interaction, represented by the tensor J, has the Hamiltonian:

$$H_J = I.2\pi.J. \tag{24}$$

For identical spins, the dipolar Hamiltonian governing magnetic coupling is:

$$H_D = -\frac{\gamma^2\hbar^2}{r^3} I_{z_1} I_{z_2} (3\cos^2\theta - 1), \tag{25}$$

where γ is the nuclear magnetogyric ratio of the spins, r is the internuclear distance, θ is the angle between internuclear vector r and the static magnetic field B_0 along the z-axis in the laboratory frame. By applying

a sequence of four $\pi/2$ pulses, dipolar coupling can be reduced or eliminated under appropriate conditions [19-21].

MAS can theoretically eliminate homonuclear dipolar couplings, practical constraints often limit its effectiveness, especially with strong ^{1}H–^{1}H interactions. In biological systems, MAS can be invasive. An alternative method is multiple-pulse line narrowing, using pulse sequences like WAHUHA to average out dipolar interactions.

The WAHUHA sequence, proposed in [22, 23] removes first-order dipolar terms in the average spin Hamiltonian, achieving efficient decoupling :

$$H_{eff} = \frac{\gamma^2\hbar^2}{r^3} I_{z_1} I_{z_2} . \frac{1}{6r} [1 \times 2\tau + 1 \times \tau - 2 \times 2\tau + 1 \times \tau] = 0, \qquad (26)$$

where τ represents the time interval between pulses. During the sequence, the magnetic moments spend equal amounts of time along each of the three principal axes. The NMR signal is sampled during one of the 2τ windows. This sequence can be combined with its mirror image to suppress angle errors, forming the MREV-8 pulse sequence [24].

WAHUHA. The multiple-pulse WAHUHA sequence used in the experiments was generated using the standard pulse programming rules in Bruker's Topspin software. The specific details of pulsing, timing, looping, and phasing are shown in Fig. S1.

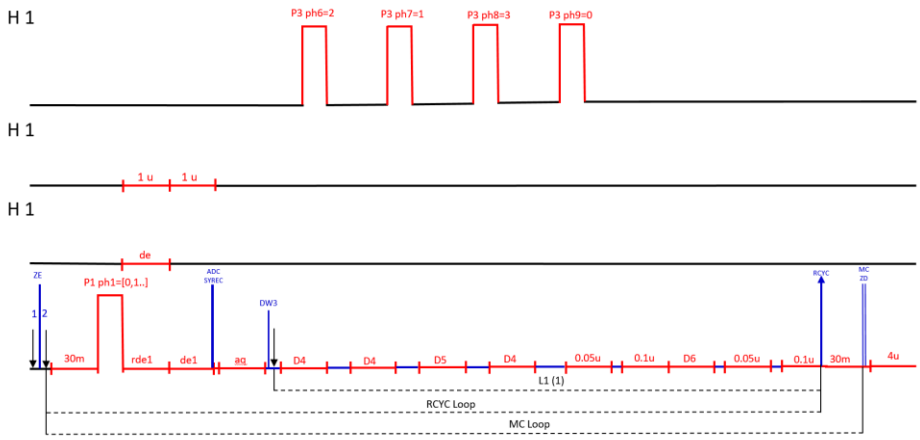

Figure S1: Schematic representation of the multiple-pulse WAHUHA sequence implemented using the AU programming language of Bruker.

The parameters conform to standard Bruker nomenclature: "D" indicates delay time in microseconds (e.g., D4, D5, D6), "P" represents the applied radiofrequency (r.f.) pulse, and "ph (1…n)" denotes the phase of the

applied r.f. pulse. "H1" designates the proton channel, "RECY loop" indicates looping, and "u" signifies the unit in microseconds. The notation "30m" stands for a duration of 30 milliseconds.

Before applying the sequence of π/2 pulses with acquisitions, there is a 30 ms delay. Correction times in microseconds are added to the waiting times to achieve refocusing. At the end of the first loop, there is another 30 ms delay before starting the looping process again (MC loop). Looping is divided into three types based on the starting time: L1, RECY loop, and MC loop. This division is essential for achieving final refocusing and preventing additional broadening.

S6. Optimal Control Pulse Optimization

Optimal control pulses can exhibit variable, noise-like shapes, which may cause distortion and reduced fidelity if the hardware is not perfectly linear. To address this, smoothness constraints were applied by filtering the pulses at each iteration and suppressing components far from resonance. Suppressing non-resonant components reduced both the total energy consumption and the specific absorption rate. This was demonstrated through pulse shapes designed to selectively excite phenylalanine (Phe) while avoiding excitation of taurine (Tau), and vice versa, at two distinct NMR frequencies: 600.13 MHz (Fig. S2a) and 29.93 MHz (Fig. S2b). The precision of the pulse design is emphasized by the observed 2 rad phase jump, a critical feature in the optimization process.

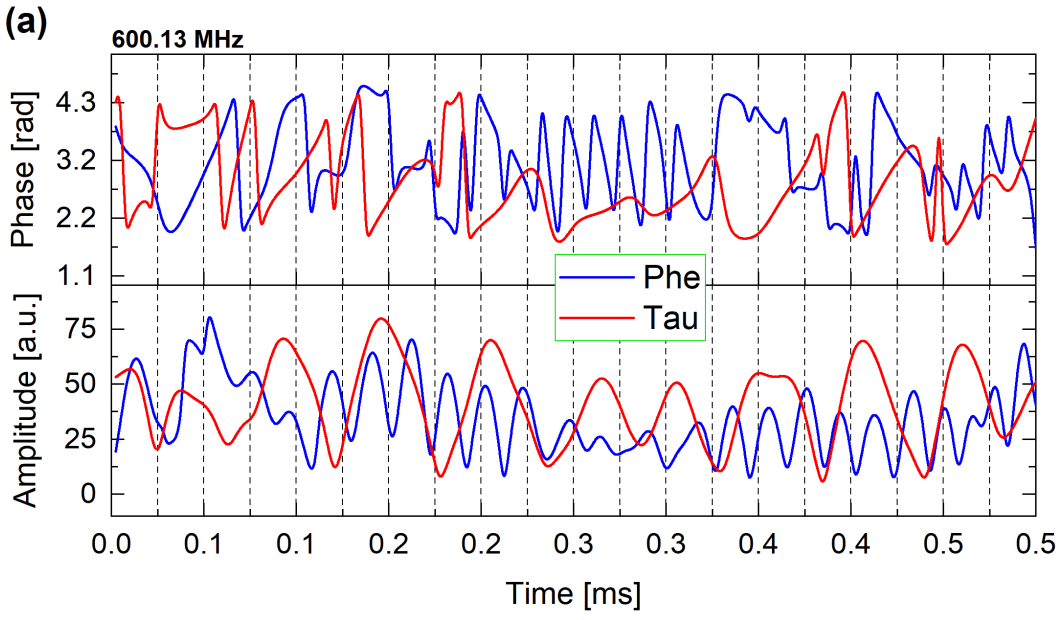

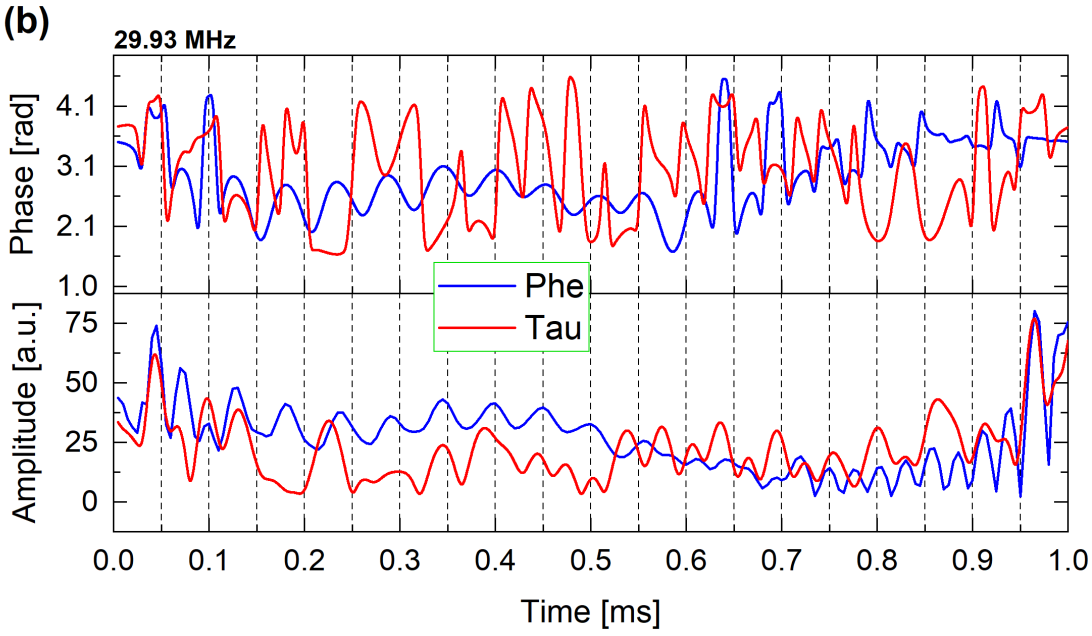

Figure S2: Pulse shapes (amplitude and phase) of the optimal controlled pulses to selectively excite Phe and Tau molecules at **(a)** low-field NMR (29.93 MHz) and **(b)** high-field NMR (600.13 MHz).

S7. Comparative Analysis of Water Suppression Techniques in Low-Field NMR

To emphasize the importance of achieving consistent NMR signals after water suppression, particularly in low-field NMR where challenges are more significant than in high-field NMR, we analyzed a phenylalanine and taurine (Phe-Tau) metabolite mixture under various conditions. The results are presented in Fig. S3 for comparative analysis. Fig. S3a shows the NMR spectrum obtained using hard pulse excitation without water suppression. In this case, a dominant water signal completely obscures other spectral features, making it impossible to extract spectral information or perform quantitative analysis of Phe and Tau metabolites. Figure A1b presents the spectrum acquired using hard pulse excitation combined with a pre-saturation water suppression routine. While the water signal is significantly reduced, residual effects remain. Notably, signals in the -30 Hz range, which are close to the water signal, experience noticeable attenuation, affecting the quantitative accuracy of Phe and Tau measurements. In contrast, signals around -52 Hz and 69.5 Hz are less affected, but the overall spectral quality is still compromised. Fig. S3c depicts the spectrum of the same sample dissolved in pure D_2O, where the water signal is eliminated without requiring additional suppression techniques. This approach provides clear and distinct Phe and Tau signals, with amplitude ratios comparable to those obtained using optimal control pulses for water suppression. While pre-saturation water suppression techniques can effectively reduce the water signal, they often result in longer acquisition times and introduce delays between successive

measurements. These delays are particularly problematic for in-situ NMR studies, where rapid data acquisition is critical. To address these limitations, we developed a non-invasive water suppression method using optimal control pulses for selective excitation.

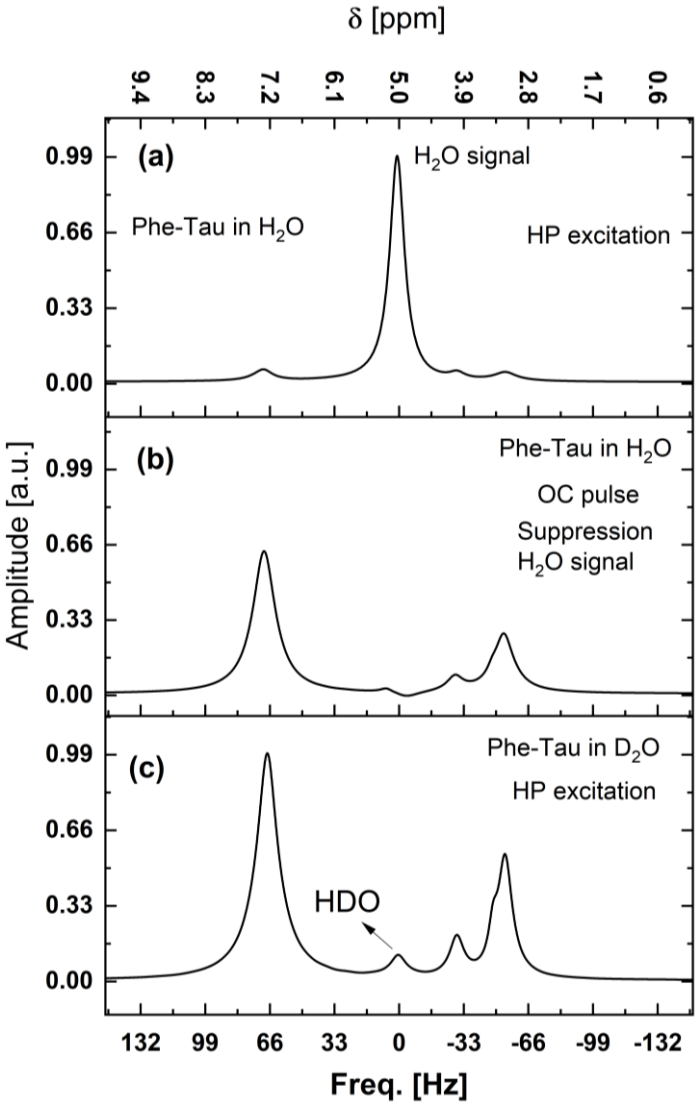

Figure S3: ^{1}H-NMR spectra of Phe-Tau in H_2O-D_2O (with 10% D_2O) recorded at a frequency of 29.93 MHz. The NMR spectra were acquired using **(a)** hard pulse excitation, **(b)** hard pulse excitation with included water suppression, and **(c)** hard pulse excitation of the same Phe-Tau system, dissolved in pure D_2O to eliminate the water signal for comparative analysis.

S8. Excitation and Suppression Factors (EF and SF)

Excitation and suppression factors (EF and SF) were calculated for Gaussian and optimal control (OC) pulses by normalizing the absolute integration of target and interfering signals to their values after excitation with a hard pulse. The results are summarized in Table S1.

Table S1: EF and SF for Gaussian and OC Pulses.

Factor	Phenylalanine		Taurine	
	OC (Krotov)	Gaussian	OC (Krotov)	Gaussian
EF	0.78	0.55	0.77	0.53
SF	0.05	0.02	0.04	0.03

Key observations reveal that suppression factors (SF) for both pulse types were comparable, with values averaging around 0.03. However, excitation factors (EF) indicated that OC pulses were more efficient, achieving higher values (~0.78) compared to Gaussian pulses (~0.54).

References

[1] M. Guéron, P. Plateau, and M. Decorps, "Solvent signal suppression in NMR," *Progress in nuclear magnetic resonance spectroscopy,* vol. 23, no. 2, pp. 135-209, 1991.

[2] M. Canton, R. Roe, S. Poigny, J.-H. Renault, and J.-M. Nuzillard, "Multiple solvent signal presaturation and decoupling artifact removal in 13 C {1 H} nuclear magnetic resonance," *Magnetic Resonance,* vol. 1, no. 2, pp. 155-164, 2020.

[3] L. M. Botana, *Seafood and freshwater toxins: pharmacology, physiology, and detection*. Crc Press, 2014.

[4] A. S. Altieri and R. A. Byrd, "Randomization approach to water suppression in multidimensional NMR using pulsed field gradients," *Journal of Magnetic Resonance, Series B,* vol. 107, no. 3, pp. 260-266, 1995.

[5] T.-L. Hwang and A. Shaka, "Water suppression that works. Excitation sculpting using arbitrary wave-forms and pulsed-field gradients," *Journal of Magnetic Resonance, Series A,* vol. 112, no. 2, pp. 275-279, 1995.

[6] T. Castaing-Cordier, D. Bouillaud, P. Bowyer, O. Gonçalves, P. Giraudeau, and J. Farjon, "Highly Resolved Pure-Shift Spectra on a Compact NMR Spectrometer," *ChemPhysChem,* vol. 20, no. 5, pp. 736-744, 2019.

[7] E. R. McCarney, R. Dykstra, and P. Galvosas, "Evaluation of benchtop NMR Diffusion Ordered Spectroscopy for small molecule mixture analysis," *Magnetic resonance imaging,* vol. 56, pp. 103-109, 2019.

[8] F. Dalitz, M. Cudaj, M. Maiwald, and G. Guthausen, "Process and reaction monitoring by low-field NMR spectroscopy," *Progress in nuclear magnetic resonance spectroscopy,* vol. 60, pp. 52-70, 2012.

[9] C. P. Slichter, *Principles of magnetic resonance*. Springer Science & Business Media, 2013.

[10] C. Dybowski, "Z eeman Interaction in Nuclear Magnetic Resonance," *Encyclopedia of Analytical Chemistry: Applications, Theory and Instrumentation,* 2006.

[11] D. Grass, J. P. Caulkins, G. Feichtinger, G. Tragler, and D. A. Behrens, "Optimal control of nonlinear processes," *Berlino: Springer,* 2008.

[12] N. Khaneja, T. Reiss, C. Kehlet, T. Schulte-Herbrüggen, and S. J. Glaser, "Optimal control of coupled spin dynamics: design of NMR pulse sequences by gradient ascent algorithms," *Journal of magnetic resonance,* vol. 172, no. 2, pp. 296-305, 2005.

[13] N. Doğan, R. Topkaya, H. Subaşi, Y. Yerli, and B. Rameev, "Development of Halbach magnet for portable NMR device," in *Journal of Physics: Conference Series*, 2009, vol. 153, no. 1: IOP Publishing, p. 012047.
[14] Z. Tošner, T. Vosegaard, C. Kehlet, N. Khaneja, S. J. Glaser, and N. C. Nielsen, "Optimal control in NMR spectroscopy: Numerical implementation in SIMPSON," *Journal of Magnetic Resonance,* vol. 197, no. 2, pp. 120-134, 2009.
[15] H. Soltner and P. Blümler, "Dipolar Halbach magnet stacks made from identically shaped permanent magnets for magnetic resonance," *Concepts in magnetic resonance part a,* vol. 36, no. 4, pp. 211-222, 2010.
[16] A. C. Sauerwein, "Estimations of dipolar couplings in multiple-spin systems by solid state NMR," University of Southampton, 2010.
[17] T. Gullion and J. Schaefer, "Rotational-echo double-resonance NMR," *Journal of Magnetic Resonance (1969),* vol. 81, no. 1, pp. 196-200, 1989.
[18] J. R. Garbow and T. Gullion, "Improvements in REDOR NMR spectroscopy. Minimizing resonance-offset effects," *Journal of Magnetic Resonance (1969),* vol. 95, no. 2, pp. 442-445, 1991.
[19] T. M. Alam and J. E. Jenkins, "HR-MAS NMR spectroscopy in material science," *Advanced aspects of spectroscopy,* vol. 10, p. 279, 2012.
[20] J. S. Waugh, L. M. Huber, and U. Haeberlen, "Approach to high-resolution NMR in solids," *Physical Review Letters,* vol. 20, no. 5, p. 180, 1968.
[21] J. Farjon, W. Bermel, and C. Griesinger, "Resolution enhancement in spectra of natural products dissolved in weakly orienting media with the help of 1H homonuclear dipolar decoupling during acquisition: application to 1H–13C dipolar couplings measurements," *Journal of Magnetic Resonance,* vol. 180, no. 1, pp. 72-82, 2006.
[22] J. Waugh, L. Huber, and U. Haeberlen, "Approach to high-resolution NMR in solids," *Physical Review Letters,* vol. 20, no. 5, p. 180, 1968.
[23] J. Miller, D. Cory, and A. Garroway, "Multiple Pulse Line Narrowing: Approaches for Solid State NMR Imaging," *Review of Progress in Quantitative Nondestructive Evaluation,* pp. 649-654, 1992.
[24] P. Jackson and R. K. Harris, "A practical guide to combined rotation and multiple-pulse NMR spectroscopy of solids," *Magnetic Resonance in Chemistry,* vol. 26, no. 11, pp. 1003-1011, 1988.